Sensors and Materials, Vol. 29, No. 12 (2017) 1723–1731
MYU Tokyo

S & M 1465

A Piezoelectric Energy Harvester Utilizing $Pb[Zr_xTi_{1-x}]O_3$ Thick Film on Phosphor Bronze

Guimiao Li,[1] Bin Yang,[1*] Cheng Hou,[1,2] Gang Tang,[1,2]
Jingquan Liu,[1] Xiang Chen,[1] Xiaolin Wang,[1] and Chunsheng Yang[1]

[1]National Key Laboratory of Science and Technology on Micro/Nano Fabrication,
Department of Micro/Nano Electronics, Shanghai Jiao Tong University, Shanghai 200240, China
[2]Jiangxi Province Key Laboratory of Precision Drive & Control,
Department of Mechanical Engineering, Nanchang Institute of Technology, Nanchang 330099, China

(Received March 1, 2017; accepted May 26, 2017)

Keywords: piezoelectric energy harvester, phosphor bronze substrate, high acceleration

In this work, a bridge-type piezoelectric energy harvester combined with proof masses that can work at high acceleration was designed, simulated, and fabricated. The energy harvester was achieved by bonding bulk $Pb[Zr_xTi_{1-x}]O_3$ (PZT) onto a flexible phosphor bronze substrate by a low-temperature process, and an additional tungsten mass was assembled at the center of the bridge top surface to reduce the resonant frequency of the harvester. The device has good flexibility and is operable under high-acceleration conditions. The experimental results showed that at the resonant frequency, which is 511 Hz, the maximum open-circuit voltage is 4.72 V, when the input vibration acceleration is 8*g*. The maximum output power and output power density under 8*g* are 56.74 μW and 721.286 μW/cm^3, respectively. Additionally, we applied the fabricated device on a vacuum compression pump to test the output voltage, and found the maximum output voltage to be 0.34 V.

1. Introduction

Thanks to the rapid development of micro-electromechanical system (MEMS) technology, wireless sensor networks, wearable devices, and implantable devices are now being widely used in our daily life.[1,2] However, how to power these devices has become an issue.[3–5] Energy harvesters based on MEMS technology can convert vibration energy excited in our environment into a source of electrical energy to power these devices and has become a hot research topic of many research groups.[6–8] Compared with a traditional battery, piezoelectric MEMS-based energy harvesters have some advantages, such as miniature size, simple structure, and long lifetime.[9,10] Now, $Pb[Zr_xTi_{1-x}]O_3$ (PZT) piezoelectric ceramics are commonly used in energy harvesters to generate excellent output power owing to their high piezoelectric coefficients and electromechanical coupling.[11,12] A PZT film can be prepared by several techniques, such as sputtering, epitaxial growth, sol-gel spin on, hydrothermal method, and screen printing, which usually require high-temperature processes that restrain the film density.[13] Now, the preparation of a high-quality PZT film at low temperature using bulk PZT has been achieved.[10,14] On the other hand, a thicker and uniform PZT film will create better output power. Bulk PZT was bonded with the substrate and then ground to form a thicker PZT film. At present, piezoelectric energy

*Corresponding author: e-mail: binyang@sjtu.edu.cn
http://dx.doi.org/10.18494/SAM.2017.1586

harvesters are usually fabricated as cantilevers, which undergo large deformation when subjected to a large force in a vibration environment. Then, the application of the energy harvesters will be restricted because their encapsulation is difficult, leading to susceptibility to damage.[15] As a consequence, a bridge-type structure has been designed and prepared. The amplitude of an energy harvester is decreased because the beam is fixed at both ends.

Traditionally, piezoelectric energy harvesters are fabricated by bonding a bulk PZT film with a silicon substrate.[16,17] Failure of the device occurs owing to the brittleness of silicon when it bears a large external mechanical force or high acceleration.[4,6,18] In particular, the acceleration of a vibration source can exceed 10*g* in some production or military facilities.[19] Therefore, it is necessary for those energy harvesters to be operable under high-acceleration or massive-impact conditions. In our study, phosphor bronze substrate is utilized as the bonding substrate owing to its flexibility and elasticity, which will broaden the application range and improve the reliability of the harvester. Moreover, the vibration frequency of excitation sources would vary from one case to another.[18,20]

In this paper, we propose a bridge-type piezoelectric energy harvester fabricated by the standard MEMS technique including the thinning and polishing of bulk PZT by mechanical grinding as well as the formation of a silicon proof mass by deep reactive-ion etching (DRIE) methods. The energy harvester is operable at high acceleration. The microfabrication process of the bridge-type piezoelectric energy harvester is illustrated. Finally, the fabricated harvester performance is experimentally tested.

2. Design and Fabrication

2.1 Design of energy harvester

In accordance with our design, we proposed a bridge-type structure of the energy harvester in order to realize a small amplitude under high acceleration. Thus, the energy harvester can work at high acceleration. The structure mainly includes a piezoelectric functional layer, conductive epoxy adhesive layer, phosphor bronze substrate supporting layer, and proof masses of integrated silicon and assembled tungsten. Figure 1(a) shows the cross-sectional diagram of the harvester. In order to simplify the simulation process, a surrogate model was set up as shown in Fig. 1(b). The

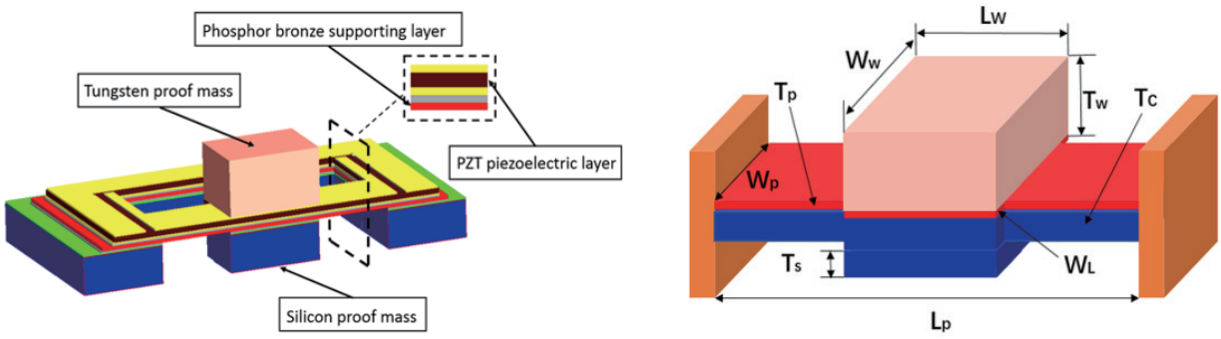

(a) (b)

Fig. 1. (Color online) (a) Cross-sectional image and (b) simplified model of the device.

dimensions of the designed energy harvester are given in Table 1. The result of the finite element method (FEM) modeling simulation by ANSYS is shown in Fig. 2. The 1st and 2nd resonant frequencies are 583.98 and 796.34 Hz, respectively. Simultaneously, it can be seen that the bridge-type structure generates the twisted deformation at the resonant frequency.

2.2 Fabrication of energy harvester

The energy harvester was achieved by bonding bulk PZT onto a flexible phosphor bronze substrate by a low-temperature process and manufacturing a piezoelectric layer by the standard MEMS technique. An additional tungsten mass was assembled at the center of the bridge top surface for the sake of reducing the resonant frequency of the harvester.

The main fabrication process comprises the bonding, mechanical thinning, and polishing of bulk PZT, bridge structure patterning, and proof mass forming by DRIE methods. Note that when a piezoelectric material is heated to its Curie temperature, it will be completely depolarized.

Table 1
Dimensions of the designed energy harvester.

Structural layers	Geometrical parameters (μm)	Value
Phosphor bronze	Length (L_p)	12000
	Width (W_p)	3000
	Thickness (T_c)	90
PZT	Length (L_p)	12000
	Width (W_p)	3000
	Thickness (T_p)	50
Silicon proof mass	Length (L_w)	5000
	Width (W_w)	5000
	Thickness (T_s)	400
Tungsten proof mass	Length (L_w)	5000
	Width (W_w)	5000
	Thickness (T_w)	25000

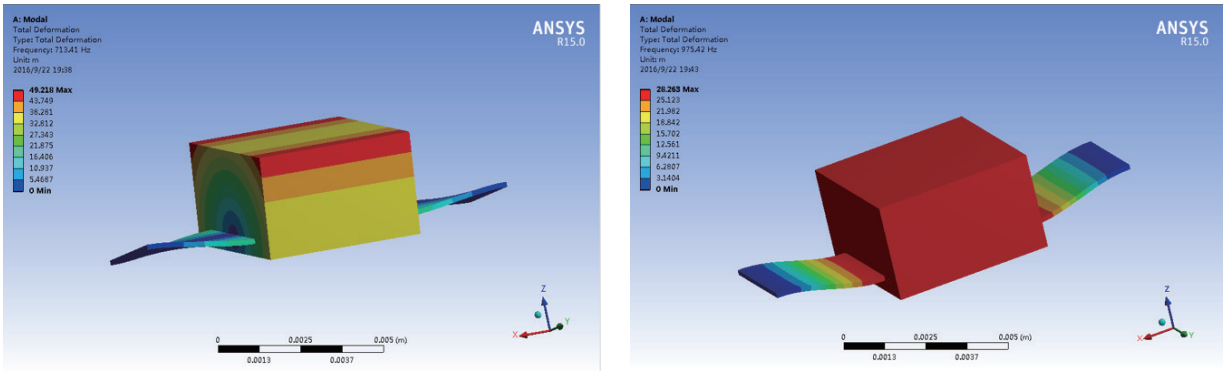

(a) (b)

Fig. 2. (Color online) FEM simulation of this device under (a) 1st resonant frequency of 583.98 Hz and (b) 2nd resonant frequency of 796.34 Hz.

Hence, the whole process must be accomplished at low temperature. The piezoelectric layer used in this work is PZT-6C (provided by FUJI Ceramics Corporation), and its Curie temperature is about 295 °C. The specific fabrication process is described in Fig. 3. The process begins with a 400-μm-thick silicon substrate, and a 2-μm-thick plasma-enhanced chemical vapor deposition (PECVD) SiO_2 film is deposited on one side to provide electrical isolation of silicon [Fig. 3(a)]. Then, a 100-μm-thick phosphor bronze substrate (provided by Shanghai Yongtai Mechanical and Electrical Corporation) is bonded with the silicon substrate at 90 °C using 504 glue, and the thickness of the glue is about 4 μm. In order to obtain a more slippery surface for enhancing the adhesion of bulk PZT with the phosphor bronze substrate, the latter is thinned and polished by mechanical lapping to a thickness of 90 μm [Fig. 3(b)]. Later, 200-nm-thick Cr/Au was sputtered as the bottom electrode onto one side of the PZT film. The conductive epoxy (provided by Shanghai Research Institute of Synthetic Resins) was coated by screen printing as an intermediate layer for bonding bulk PZT with phosphor bronze substrate in vacuum at 175 °C (3 h). The bonding pressure of the process is about 0.1 MPa and the thickness of the intermediate layer is about 4 μm [Fig. 3(c)]. The bulk PZT is thinned down to about 40 μm by mechanical lapping and polishing in order to improve the adhesion between the PZT film and the top electrode, and the roughness of its surface should be controlled to less than 30 nm [Fig. 3(d)]. The top electrode is also formed by sputtering 200-nm-thick Cr/Au. Afterwards, top and bottom electrodes are divided by ion beam milling [Figs. 3(e) and 3(f)]. The back of the silicon proof mass is formed by lithography followed by reactive-ion etching (RIE) and DRIE. The bridge-type structure is patterned by ultraviolet irradiation from the backside, which can avoid the ablation of the top electrode [Fig. 3(g)]. The

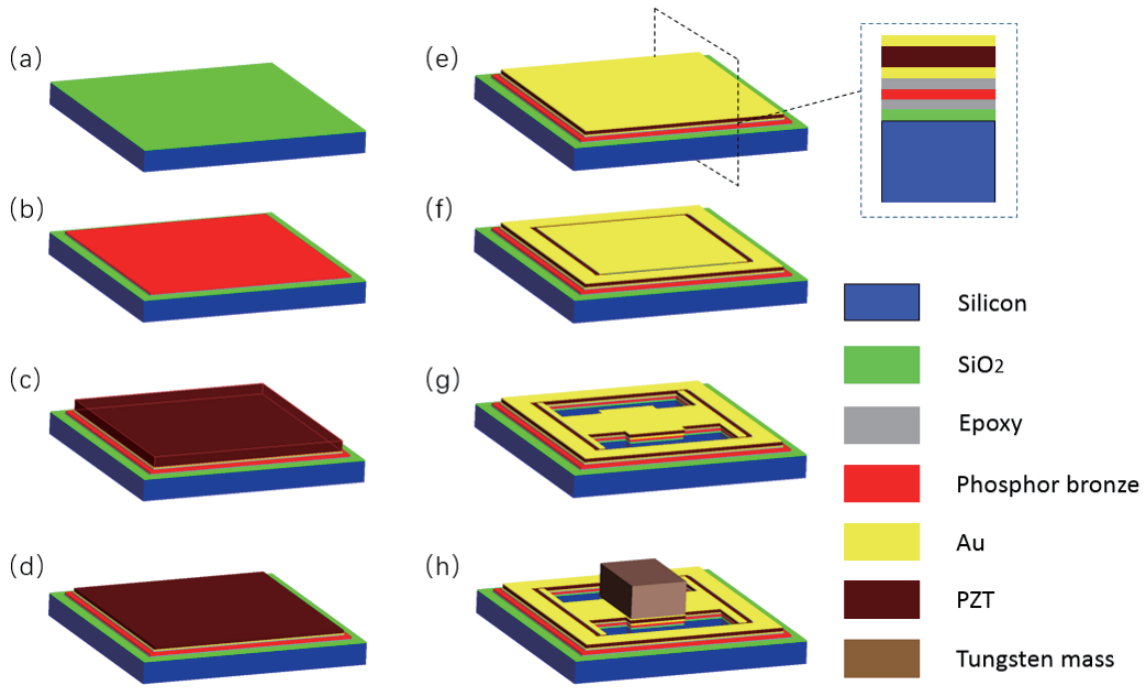

Fig. 3. (Color online) Fabrication process of energy harvester.

additional tungsten mass is assembled at the center of the bridge top surface to further reduce the resonant frequency of this device [Fig. 3(h)]. The fabricated bridge-type piezoelectric energy harvester is shown in Fig. 4. In addition, the bulk PZT after thinning and polishing, as well as the cross-sectional image of the device, was analyzed by SEM. Figure 4(b) indicates that there are no obvious holes or scratches, which means that the PZT film has high uniformity. The structure of the bridge-type piezoelectric energy harvester is clearly shown in Fig. 4(c), and there is a distinct conductive epoxy adhesive layer between the piezoelectric layer and the supporting layer. Both sides of the bridge-type structure are attached to acrylic using adhesive to fix the device. Figure 5 shows the phase angle of the fabricated device versus the exciting frequency measured using an impedance analyzer (Keysight E4990A). The 1st and 2nd resonant frequencies of the bridge energy harvester are 563 and 751 Hz, respectively. There is good agreement between the FEM simulation and experimental results.

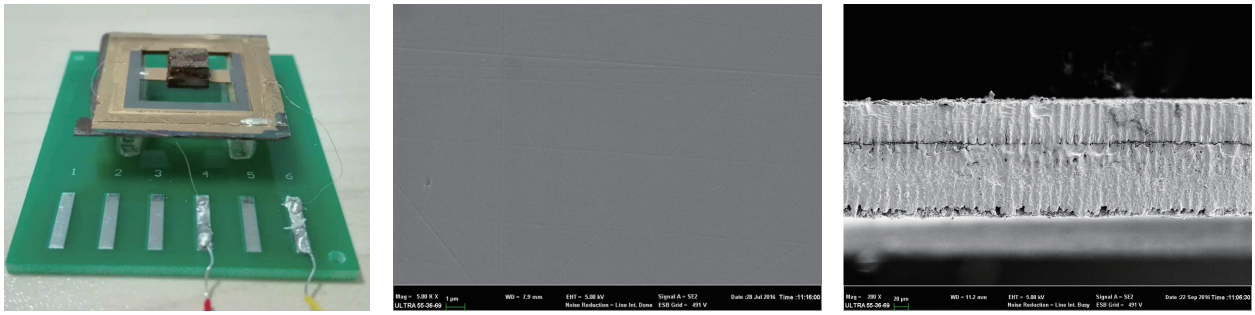

(a) (b) (c)

Fig. 4. (Color online) (a) Fabricated bridge piezoelectric energy harvester. (b) SEM image of the PZT surface after lapping and polishing. (c) Cross-sectional view of the composite cantilever.

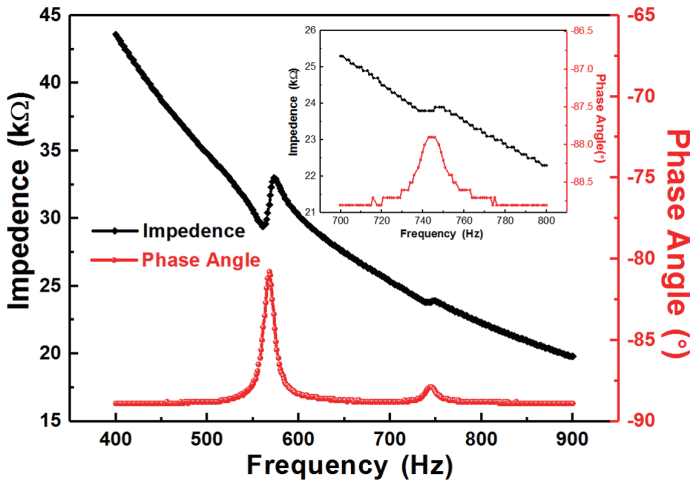

Fig. 5. (Color online) Resonant frequency of the bridge energy harvester.

3. Testing and Characterization of Energy Harvester

3.1 Testing platform

The performance of the bridge-type energy harvester was investigated using the experimental setup given in Fig. 6(a), which includes a signal generator, a power amplifier, a shaker simulating the vibration source, an accelerometer, and an oscilloscope. The signal was generated by the signal generator and amplified by the power amplifier to control the vibration of the energy harvester mounted on the shaker platform, while the vibration acceleration was monitored by the accelerator attached to the shaker. The electrical output of the energy harvester under different vibration conditions was monitored with the oscilloscope.

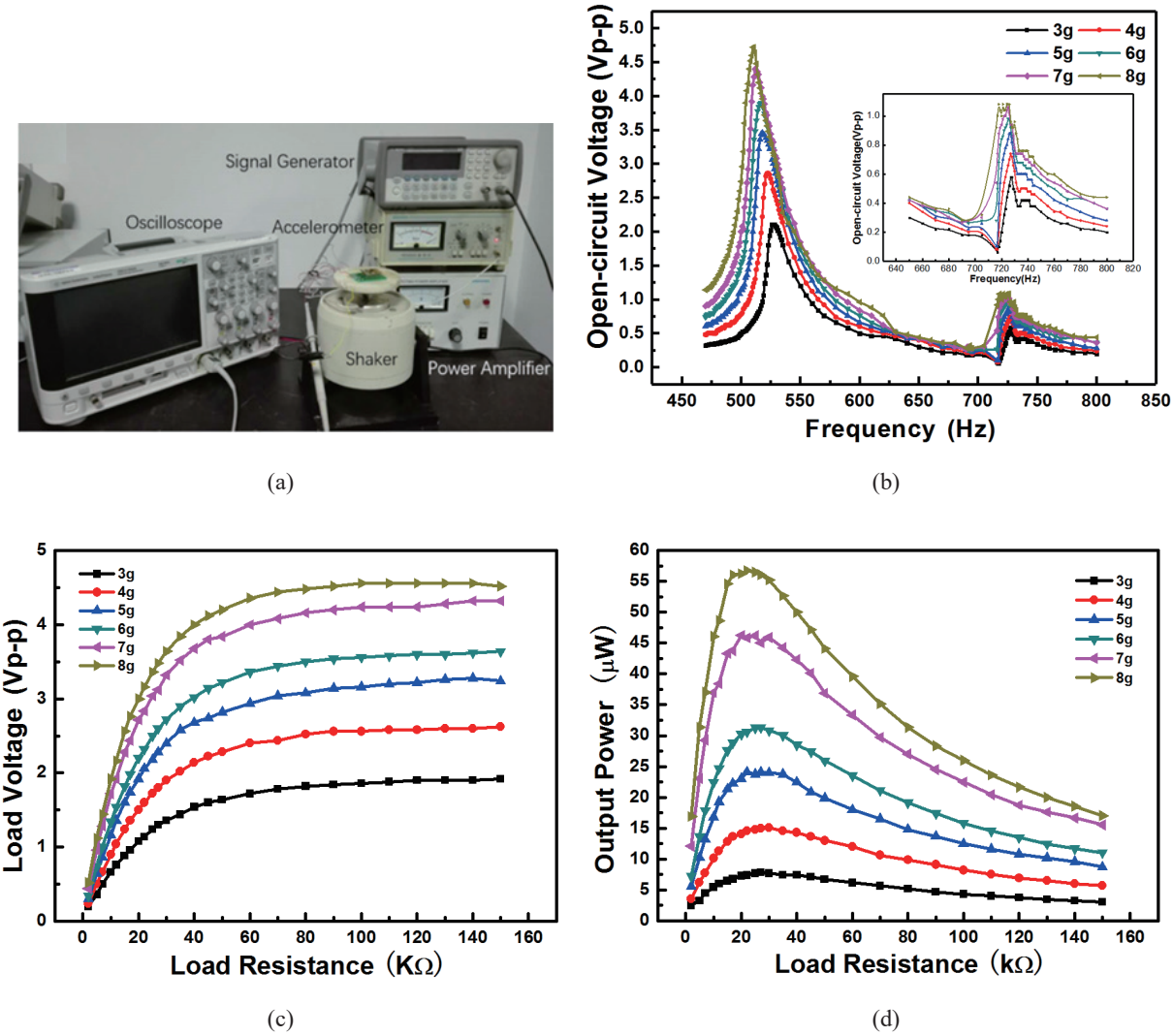

Fig. 6. (Color online) (a) Test setup of energy harvester. (b) Measured open-circuit voltage. (c) Output load voltage under different load resistances. (d) Output power for different load resistances.

3.2 Characterization and discussion

After the test, the open-circuit voltage and loading voltage are shown in Figs. 6(b) and 6(c), respectively, under different resistances at accelerations from 3*g* to 8*g*. The maximum open-circuit voltages were increased following the augmentation of input vibration acceleration. At the 1st resonant frequency, the maximum open-circuit voltages are 2.1, 2.86, 3.46, 3.9, 4.4, and 4.72 V, when the input vibration acceleration is increased from 3*g* to 8*g*. At the 2nd resonant frequency, the maximum open-circuit voltages are 0.58, 0.74, 0.88, 0.98, 1.06, and 1.08 V when the input vibration acceleration is increased from 3*g* to 8*g*. Most energy harvesters can only work under 5*g*, so these results suggest that our energy harvester is operable at high acceleration without incurring any damage. Figure 6(b) shows that when the acceleration of the vibration source is increased, the resonant frequency of the energy harvester is also decreased. The reason for this decrease was the increase in the damping ratio with acceleration owing to the nonlinearity of PZT under large stress.[21] At the 1st resonant frequency, the structure generates the twisted deformation first owing to the extra-high proof mass.

Under the resonant frequencies, the output power will become maximum when the load resistance matches the resistance of the device. As Fig. 6(c) shows, the load voltage increased with increasing acceleration. Under a certain acceleration, the load voltage increases with the increase in the load resistance. The increasing trend is greater at a lower load resistance than at a higher load resistance.

The output average power can be calculated using

$$P = [V_{P-P}/(2\sqrt{2})]^2/R, \tag{1}$$

where V_{P-P} is the loading voltage of the peak-to-peak value, and R is the load resistance.

On the basis of Eq. (1), the output power at the 1st resonant frequency for different load resistances is shown in Fig. 6(d). It is observed that the maximum output power and output power density under 8*g* are 56.74 μW and 721.286 μW/cm^3, respectively. The output power curve tends to increase initially and subsequently decreases when the load resistance surpasses 30 kΩ, which indicates that the matched optimal resistance is 30 kΩ.

To supervise its application in daily life, we demonstrated the energy harvester applied to a vacuum compression pump. The output voltage of the fabricated device tested on the vacuum compression pump is shown in Fig. 7(a). Figures 7(b) and 7(c) show the output voltage within 100 and 0.06 s, respectively, and the obtained maximum output voltage is 0.34 V. Despite the output performance being unsatisfactory, we will optimize the resonant frequency of this harvester to match the vibration frequency of ambient sources to improve the output power in the future.

Table 2 shows the performance of the piezoelectric energy harvesters. Our device can work under 8*g* that is the highest compared with others, which can only work below 4*g*, and the power was 56.74 μW at 511 Hz. This value was the highest at such low frequency.

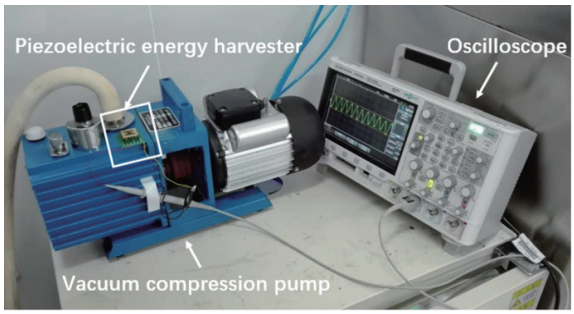

(a)

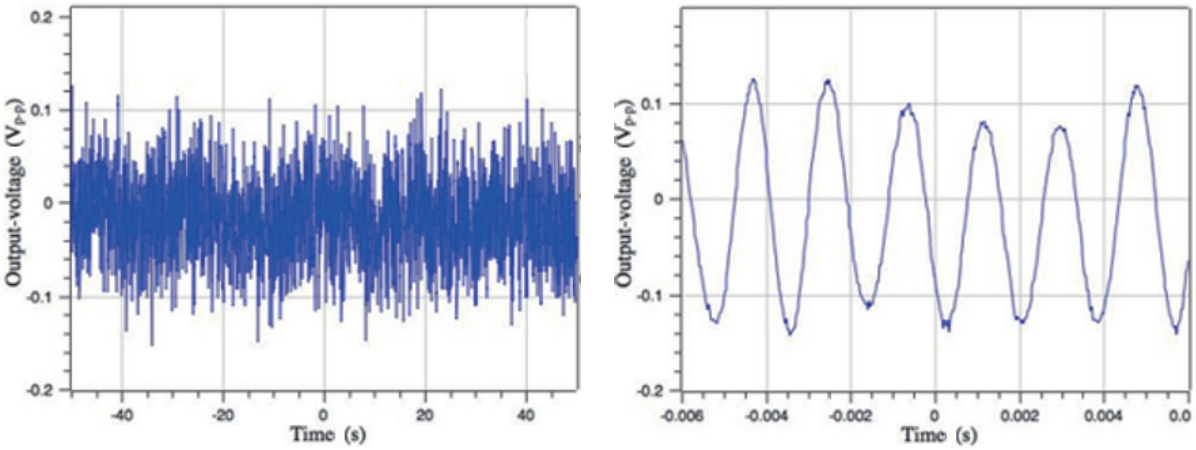

(b) (c)

Fig. 7. (Color online) Output voltage of the fabricated device tested on the vacuum compression pump.

Table 2
Comparison of recently reported performance-based piezoelectric energy harvesters.

Reference	Acceleration (*g*)	Frequency (Hz)	Power (μW)	Power Density (μW/cm^3)
Minh[23]	0.6	1960	8.6	1623
Minh[24]	1	591.6	17.7	2870
Marzencki[25]	2	2450	2.4	34
Hajati[26]	4	1350	85	582
Emad[27]	1	140	15	280.4
This work	8	511	56.74	721.286

4. Conclusions

In conclusion, we presented the fabrication of a bridge-type piezoelectric energy harvester operable at high acceleration. When the input vibration acceleration is 8*g*, the resonant frequency is 511 Hz, and the maximum open-circuit voltage is 4.72 V. At the resonant frequency, the maximum output power and output power density under 8*g* are 56.74 μW and 721.286 μW/cm^3, respectively. The matched optimal resistance is 30 kΩ. When it was tested on the vacuum compression pump, the maximum output voltage was 0.34 V. Compared with previous piezoelectric energy harvesters,

our device possesses better flexibility and resistance to larger mechanical force, which means that it can be applied to power inertial sensors in high-acceleration environments in military applications. The resonant frequency of the energy harvester can also be reduced by increasing the ratio of length to width or adding a proof mass to gain better output power.

Acknowledgments

This work was supported by the 863 Program (2015AA043503).

References

1 H. H. Huang and K. S. Chen: Sens. Actuators, A **238** (2016) 317.
2 Y. Cho, J. B. Parka, B. S. Kim, J. Lee, W. K Hong, I. K. Park, J. E. Jang, J. I. Sohn, S. N. Cha, and J. M. Kim: Nano Energy **16** (2015) 524.
3 Y. Luo, R. Y. Gan, S. L. Wan, R. L. Xu, and H. X. Zhou: AIP Adv. **6** (2016) 045319.
4 D. Shen, J. H. Park, J. H. Noh, S. Y. Cho, S. H. Kim, H. C. Wikl, and D. J. Kim: Sens. Actuators, A **154** (2009) 103.
5 Q. C. Tang and X. X. Li: IEEE/ASME Trans. Mechatronics **20** (2015) 115.
6 Y. Cui, Q. Y. Zhang, M. L. Yao, W. J. Dong, and S. Q. Gao: AIP Adv. **5** (2015) 041332.
7 D. S. Ibrahim, A. G. A. Muthalif, N. H. D. Nordin, and T. Saleh: Microsyst. Technol. **14** (2016) s00542.
8 P. Janphuang, R. Lockhart, D. Isarakorn, S. Henein, D. Briand, and N. F. de Rooij: Sens. Actuators, A **210** (2014) 1.
9 Y. C. Shu and I. C. Lien: J. Micromech. Microeng. **16** (2006) 2429.
10 H. J. Jung, H. Jabbar, Y. Song, and T. H. Sung: Sens. Actuators, A **245** (2016) 40.
11 D. J. Shin, S. J. Jeong, C. E. Seo, K. H. Cho, and J. H. Koh: Ceramics Int. **41** (2015) S686.
12 I. A. Ivan, M. Rakotondrabe, J. Agnus, R. Bourquin, N. Chaillet, P. Lutz, J. C. Poncot, R. Duffait, and O. Bauer: Rev. Adv. Mater. Sci. **24** (2010) 1.
13 K. Tanaka, T. Konishi, M. Ide, and S. Sugiyama: J. Micromech. Microeng. **16** (2006) 815.
14 X. H. Xu and J. R. Chu: J. Micromech. Microeng. **18** (2008) 065001.
15 S. Saxena, R. Sharma, and B. D. Pant: Microsyst Technol **28** (2016) s00542.
16 B. Yang, Y. B. Zhu, X. Z Wang, J. Q. Liu, X. Chen, and C. S. Yang: Sens. Actuators, A **214** (2014) 88.
17 T. Wang, T. Kobayashi, and C. K. Lee: Appl. Phys. Lett. **106** (2015) 013501.
18 S. L. Kok, N. M. White, and N. R. Harris: IEEE Sensors 2008 Conf. **44** (2008) 589.
19 J. Zhong, Y. Zhang, Q. Zhong, Q. Hu, B. Hu, and Z. L. Wang: ACS Nano **8** (2014) 6273.
20 S. L. Kok, N. Mohamad, D. F. Weng, Yap, S. Kien, Chen, and C. Fu, Dee: Int. Conf. Electrical **1** (2011) 420.
21 G. Tang, J. Q. Liu, B. Yang, J. B. Luo, H. S. Liu, Y. G. Li, C. S. Yang, D. N. He, V. D. Dao, K. Tanaka, and S. Sugiyama: J. Micromech. Microeng. **22** (2012) 065017.
22 L. V. Minh, M. Hara, and H. Kuwano: MEMS **1** (2014) 397.
23 L. V. Minh, T. Sano, T. Fujii, and H. Kuwano: PowerMEMS **773** (2016) 012003.
24 M. Marzencki, M. Defosseux, and S. Basour: J. Microelectromech. Syst. **18** (2009) 1444.
25 A. Hajati and S. G. Kim: Appl. Phys. Lett. **99** (2011) 1301.
26 A. Emad, M. A. E. Mahmoud, M. Ghoneima, and M. Dessouky: Smart Mater. Struct. **25** (2016) 11500.